



Supplementary Materials for

Structure of V-ATPase from mammalian brain

Yazan M. Abbas, Di Wu, Stephanie A. Bueler, Carol V. Robinson, John L. Rubinstein

Correspondence to: john.rubinstein@utoronto.ca

This PDF file includes:

Materials and Methods
Captions for Tables S1 to S5
Caption for Movie S1
Table S6
Figs. S1 to S14
References 57-78

Other Supplementary Materials for this manuscript include the following:

Tables S1 to S5
Movie S1

Materials and Methods

Construction, expression, and purification of a 3×FLAG tagged fragment of SidK

A plasmid bearing the *Legionella pneumophilla* gene for SidK with an N-terminal 6×histidine tag followed by a tobacco etch virus (TEV) cleavage site (19) was further modified by the Gibson assembly method to introduce a 3×FLAG tag and stop codon after residue 278, creating plasmid pSAB35. For isolation of SidK₁₋₂₇₈-3×FLAG, BL21 Codon+ cells were transformed with pSAB35 and grown at 37 °C with shaking in 2 L LB media supplemented with 0.4 % (w/v) glucose and 50 mg/L kanamycin. At an OD₆₀₀ of 0.65, protein expression was induced with 1 mM IPTG and cells were grown overnight at 16 °C. All subsequent steps were performed at 4 °C. Cells were harvested by centrifugation at 5,250 ×g and lysed by sonication in HisTrap Buffer (50 mM Tris-HCl pH 7.4, 25 mM imidazole, and 300 mM NaCl). Cell lysate was centrifuged at 38,000 ×g and the supernatant was loaded onto a 5 mL HisTrap Ni-NTA column (GE Healthcare). The column was washed with HisTrap Buffer and protein eluted with a linear gradient of imidazole from 25 to 300 mM in HisTrap Buffer over 10 column volumes (CV). Fractions containing 6×his-SidK₁₋₂₇₈-3×FLAG were pooled, mixed with TEV protease, and dialyzed against 2 L Dialysis Buffer (50 mM Tris-HCl pH 7.4 and 300 mM NaCl) with 1 mM dithiothreitol (DTT) overnight. Cleaved protein was dialyzed in 2×1 L Dialysis Buffer and passed through a 5 mL HisTrap column. The column was washed with HisTrap Buffer and the flow through and wash were collected, pooled, and exchanged into buffer containing 50 mM Tris-HCl pH 7.4, 300 mM NaCl, and 1 mM DTT by concentration and dilution in a centrifugal concentrating device (EMD Millipore). SidK₁₋₂₇₈-3×FLAG was further purified with a Superdex 75 10/300 gel filtration column (GE Healthcare) equilibrated with buffer (50 mM Tris-HCl pH 7.4 and 150 mM NaCl). Fractions containing protein were pooled, concentrated, flash frozen in liquid N₂, and stored at -80 °C.

Isolation of V-ATPase from rat brain

Membranes enriched for synaptic vesicles were collected from adult Norwegian rat brains (20). Working at 4 °C and with ice-cold buffers, two intact brains (~2.2 g each) were washed 2 to 3 times with Homogenization Buffer (320 mM sucrose, 4 mM HEPES pH 7.4), diced into cubes ~15 mm³, and transferred into Homogenization Buffer supplemented with 0.2 mM PMSF (20

mL buffer/brain). Each brain was homogenized separately with ten strokes of a Potter-Elvehjem tissue homogenizer, pooled, and centrifuged twice at 1,000 $\times g$ for 10 min with the supernatant collected and the pellet discarded. The partially clarified homogenate was centrifuged at 110,000 $\times g$ for 40 min to collect membranes. The membrane pellet was resuspended with a Dounce homogenizer in ~14 mL Solubilization Buffer (50 mM Tris-HCl pH 7, 320 mM sucrose, 300 mM NaCl, 10 % [v/v] glycerol, 5 mM ϵ -amino-n-caproic acid, 5 mM p-aminobenzamidine, 5 mM EDTA, and 0.2 mM PMSF). Resuspended membranes were flash frozen in liquid N₂ and stored at -80 °C. Frozen membranes were thawed, diluted with 38 mL of Solubilization Buffer and 2 mL of 20 % (w/v) dodecylmaltoside (DDM) in water was added and the mixture incubated for 30 min with gentle shaking. Insoluble material was removed by centrifugation for 70 min at 130,000 $\times g$. Frozen SidK₁₋₂₇₈-3 \times FLAG (1 mg) was thawed and diluted in 3 mL TBSG (50 mM Tris-HCl pH 7, 300 mM NaCl, and 10 % [w/v] glycerol), and 1 mL of this solution applied to each of three columns containing 800 μ L M2 Agarose beads (Sigma), previously equilibrated with TBSG. The columns were washed with five CVs of DTBSG (TBSG supplemented with 0.03 % [w/v] DDM). After centrifugation, the solubilized membranes were filtered with a 0.45 μ m syringe filter, divided into three pools, and applied to the three M2 Agarose columns with bound SidK₁₋₂₇₈-3 \times FLAG. The flow through of each column was collected, pooled, and passed over the columns again. This process was repeated three more times for a total of five column applications. The columns were washed with ten CVs of DTBSG and V-ATPase with SidK₁₋₂₇₈-3 \times FLAG was eluted with three CVs of DTBSG with 150 μ g/ml 3 \times FLAG peptide, followed by one CV of DTBSG. Eluted protein was pooled and concentrated to with a 100 kDa MWCO centrifuge concentrator (EMD Millipore). To remove glycerol and excess SidK₁₋₂₇₈-3 \times FLAG prior to cryoEM, the protein solution was diluted with DTBS (DTBSG without glycerol), and concentrated again to ~10 mg/ml. For protein analysed by mass spectrometry, gel filtration was performed with a Superose 6 Increase 10/300 column (GE Healthcare) equilibrated with buffer DTBSG. This additional procedure did not improve the appearance of V-ATPase particles by cryoEM or the apparent purity of the sample on an SDS-PAGE gel and was therefore omitted prior to preparation of the final cryoEM specimens. ATPase assays were performed as described previously (29). Gel densitometry was performed with *ImageJ* and *Plot2*.

CryoEM specimen preparation and imaging

V-ATPase at ~10 mg/ml (2.5 μ L) was applied to homemade nanofabricated EM grids with ~2 μ m holes (57) in a 35 nm thick film of gold (58, 59), previously glow-discharged in air for 2 min. Grids were blotted on both sides in a modified FEI Vitrobot mark III for 27.5 s at 4 °C and ~100 % RH before freezing in a liquid ethane/propane mixture (60). CryoEM data were collected with a Titan Krios G3 electron microscope equipped with a Falcon 3EC camera (Thermo Fisher Scientific), operated at 300 kV and automated with *EPU* software. Data were recorded with a calibrated pixel size of 1.06 Å as 60 s movies at 2 s/frame, 0.8 electron/pixel/s, and a total exposure of 42.7 electrons/Å² using a defocus range of 1.3 to 3.7 μ m.

Image analysis

All image processing steps were performed within *cryoSPARC* v2.5 (61). 6082 movies were collected and aligned with an implementation of *alignframes_lmbfgs* (62) and CTF parameters were estimated from the average of aligned frames with *CTFFIND4* (63). 459,764 single particle images were selected from the averages of aligned frames and beam-induced motion of individual particles corrected with an improved implementation of *alignparts_lmbfgs* (62). After initial rounds of ab-initio 3D classification and heterogeneous refinement, three classes corresponding to the three main rotational states of the enzyme were identified, containing 90,648, 74,789, and 79,654 particles images (Fig. S3). These 3D classes were refined with non-uniform refinement to overall resolutions of 3.9, 4.0, and 3.9 Å, respectively. Focused refinement with signal subtraction (64) targeting the membrane-embedded region, the N-terminal domain of subunit a1 with subunit C1, and the peripheral stalks excluding the detergent micelle, improved the map quality of the membrane-embedded region as well as the peripheral stalks for all three classes (V_OE₃G₃C focused refinements,). Focused refinement of the membrane-embedded region and the membrane-proximal region of subunits D and F resulted in maps at 3.8 Å, 4.2Å, and 4.4 Å resolution for state 1, state 2, and state 3, respectively (V_ODF focused refinements). Focused refinement of the A₃B₃ subcomplex and the A₃B₃-interacting portions of the central and peripheral stalks and SidK was also performed, resulting in maps at ~3.6 Å for all rotational states (A₃B₃E₃G₃DSidK₃ focused refinements,). All Fourier shell correlation (FSC) curves were calculated with independently refined half-maps and resolution was assessed at the 0.143 criterion with correction for the effects of masking maps (Fig. S4). For illustration purposes, a

composite map of rotational state 1 was generated by combining the three maps from focused refinement of rotational state 1 in UCSF chimera (65). Specifically, the three focused refinement maps were first aligned onto the non-uniform refinement map of state 1 using the ‘Fit in map’ command. Overlapping regions from each map were removed with the ‘Volume eraser’ tool. Finally, the three maps were merged with the maximum function volume operation with concurrent scaling of each map. The resulting composite map was not used for model refinement.

Construction of atomic models

An atomic model for most of rotational state 1 was built with *Coot* (66) into the 3.8 Å and 3.6 Å maps from focused refinement of state 1. For ATP6AP1/Ac45, only residues 412-452 were built as the luminal domain could not be modelled. The following regions were also not modelled: subunit A residues 1-16, subunit B2 residues 1-38 and 216-224, subunit D residues 218-247, subunit a1 residues 667 to 712, as well as short segments at the N and C termini of most subunits. To generate starting models, homology models were prepared for subunits A, B2, D, and F from *Enterococcus hirae* V₁-ATPase structure 3VR4 (31), subunit C1 from *S. cerevisiae* subunit C structure 1U7L (67), subunits E1 and G2 from *S. cerevisiae* EGC structure 4DL0 (68), and for subunits a1, c'', c, d1, e2, f, and the transmembrane α -helix of ATP6AP2/Ac45 from yeast V₀ structures 6O7U and 6C6L (9, 29). Homology models were constructed with either *phenix.sculptor* (69), *SWISS-MODEL* (70), or in *Coot* with a ‘Mutate active chain to template sequence’ script (<https://github.com/olibclarke/coot-trimmings>). The transmembrane α -helix of ATP6AP2/PRR (residues 292-343) was built *de novo*. The final model also included SidK residues 2 to 235 from a SidK crystal structure PDB 5UFK (19). Models were refined into their respective maps with *phenix.real_space_refine* using secondary structure and geometric restraints followed by manual adjustments in *Coot*. A final refinement step was performed with *Rosetta FastRelax* (71) with torsional refinement enabled. Atomic models of rotational states 2 and 3 were built by separate rigid body fitting of subunits from the rotational state 1 model into focused-refinement maps for the two different states, followed by refinement with *phenix*, *Rosetta*, and *Coot*. For rotational state 3, the C-terminal domain of subunit a1, subunit e2, and subunit f were modelled as backbone with truncated side chains. To build the membrane proximal portions of subunits E1 and G2, the N-terminal domain of subunit a1, and subunit C1,

homology models for these proteins were fit into the map from the 4.3 Å focused refinement of rotational state 1 using *Coot* all-atom refine with PROSMART all-molecule restraints enabled followed by refinement with *Rosetta FastRelax*. To ensure that the proper helix register is maintained within the peripheral stalks, the membrane-distal C-terminal domains of E1 and G2 were kept intact during building and refinement, but were then removed as these regions overlapped with the model from the A₃B₃E₃G₃DSidK₃ focused refinement. The final model for this region contained only backbone with truncated side chains, and lacks subunit a1 residues 133-169 and subunit C1 residues 348-362. This model was then fit into the corresponding focused refinement maps of rotational states 2 and 3 using *Coot* and refined with *Rosetta* and *phenix* as described for state 1. Models were validated with *MolProbity* (72) and *EMRinger* (73).

For illustration purposes and to generate the movie, composite models for each rotational state were generated as follows. The focused refinements maps from each state were aligned onto the corresponding non-uniform refinement in UCSF Chimera using the ‘Fit in map’ command. Models built using focused refinements maps were then rigid body fit into the realigned maps in *coot* and subsequently merged. No further refinement of the composite models was performed. Figures and the movie were generated with *UCSF ChimeraX* (74) or *UCSF Chimera* (65).

Mass spectrometry and bioinformatics

For the identification of protein subunits, affinity purified V-ATPase was further purified with a Superose 6 Increase 10/300 column (GE Healthcare) equilibrated with DTBSG. Fractions containing the enzyme were pooled, concentrated to 4 mg/ml, flash frozen in liquid N₂, and stored at -80 °C prior to analysis. The sample was subjected to SDS-PAGE with a NuPAGE 4 to 12 % Bis-Tris gel in MES buffer (Thermo Fisher Scientific) that was subsequently cut into fourteen contiguous gel regions (Fig. S1A). Proteins were digested in the gel as described previously (75) with trypsin at 37 °C or chymotrypsin at 25 °C. Peptides were dissolved in 0.1 % (v/v) TFA and 5 % (v/v) DMSO and separated by nano-flow liquid chromatography (EASY nLC 1000, Thermo Fisher Scientific; mobile phase A: 0.1 % [v/v] formic acid; mobile phase B: 100 % [v/v] acetonitrile, 0.1 % [v/v] formic acid). Peptides were then loaded onto a trap column (5 mm PepMap RSCL C18, 300 µm inner diameter, particle size 5 µm; Thermo Fisher Scientific) and eluted with a gradient of 5 to 90 % (v/v) mobile phase B over 30 min. Separated peptides

were eluted directly into a Q Exactive Orbitrap Mass Spectrometer (Thermo Fisher Scientific). Typical mass spectrometric conditions were: spray voltage of 1.8 kV; capillary temperature of 320 °C. The Q Exactive Orbitrap Mass Spectrometer was operated in data-dependent mode. Survey full-scan MS spectra were acquired in the orbitrap (m/z 350 to 1500) with a resolution of 70000 and an automatic gain control target at 3×10^6 . The top ten most intense ions were selected for higher-energy collisional dissociation MS/MS fragmentation in the orbitrap at a resolution of 17500. Raw files were converted into mgf files using raw2msm software (76). Mgf files were searched against the Uniprot *Rattus norvegicus* database with the Mascot search engine v2.5.1 (Matrix Science). Search parameters were: peptide mass tolerance, 10 ppm; fragment mass tolerance, 0.2 Da; enzyme, trypsin or chymotrypsin as appropriate; missed cleavage sites, up to 2; fixed modification, carbamidomethylation (cysteine) and variable modification, oxidation (methionine). To assess the relative abundance of cleaved versus intact ATP6AP1/Ac45 and cleaved versus intact ATP6AP2/PRR, the integrated intensity of chromatography peaks were compared for identical peptides from gel regions corresponding to the cleaved and intact forms of the proteins. Identification of RNaseK as a homolog of yeast subunit f was done with PSI-BLAST (77). Exponentially modified protein abundance index (emPAI) scores were calculated as described previously (78). For native MS analysis of intact V-ATPase, the protein sample was buffer exchanged to 200 mM ammonium acetate, 0.02 mM lauryl maltose neopentyl glycol (LMNG), pH 7.0 and analyzed on a Q Exactive UHMR mass spectrometer (Thermo Fisher Scientific). Typical native mass spectrometric conditions were: spray voltage of 1.1 kV; capillary temperature of 250 °C, HCD collisional energy of 50 to 250 V.

Table S1. Mass spectrometry of tryptic peptides.

Table S2. Top ten identified proteins for each gel band.

Table S3. Mass spectrometry of subunits e2, ATP6AP1/Ac45, ATP6AP2/PRR, and RNaseK.

Table S4. Other V-ATPase subunit isoforms detected in preparation.

Table S5. V₁ region mass calculation.

Table S6. CryoEM map and atomic model statistics.

Cryo-EM maps	Focused A ₃ B ₃ E ₃ G ₃ DSidK ₃			Focused V ₀ DF			Focused V ₀ E ₃ G ₃ C			Overall non-uniform refinement		
	State 1	State 2	State 3	State 1	State 2	State 3	State 1	State 2	State 3	State 1	State 2	State 3
EMDB ID	21345	21346	21347	21348	21349	21350	21351	21352	21353	21317	21318	21319
Particle images contributing to maps	90,648	74,789	79,654	90,648	74,789	79,654	90,648	74,789	79,654	90,648	74,789	79,654
Global resolution (FSC = 0.143, Å)	3.6	3.7	3.6	3.8	4.2	4.4	4.3	5.7	5.7	3.9	4.0	3.9
Model Building	Focused A₃B₃E₃G₃DSidK₃			Focused V₀DF			Focused V₀E₃G₃C					
Associated PDB ID	6VQ9	6VQA	6VQB	6VQC	6VQG	6VQH	6VQI	6VQJ	6VQK			
Modelling and refinement software	<i>Coot, Phenix, Rosetta</i>			<i>Coot, Phenix, Rosetta</i>			<i>Coot, Phenix, Rosetta</i>					
Protein residues	4578	4578	4578	2813	2813	2813	1062	1062	1062			
Ligand	1 Mg-ADP	1 Mg-ADP	1 Mg-ADP	-	-	-	-	-	-			
RMSD bond length (Å)	0.01	0.01	0.01	0.008	0.008	0.008	0.004	0.006	0.005			
RMSD bond angle (°)	0.89	0.88	0.88	0.97	0.98	1.00	1.12	1.34	1.25			
Ramachandran outliers (%)	0.18	0.20	0.20	0.22	0.25	0.22	0.48	0.19	0.10			
Ramachandran favoured (%)	97.09	97.11	97.18	97.11	97.22	97.22	98.17	98.94	98.46			
Rotamer outliers (%)	0.10	0.05	0.05	0.56	1.36	2.06	0.00	0.00	0.00			
Clash score	1.01	1.52	1.36	3.56	5.11	5.07	2.47	4.17	5.73			
MolProbity score	0.96	1.05	1.02	1.31	1.52	1.65	1.03	1.20	1.31			
EMRinger score	2.13	2.12	1.92	1.76	1.02	0.43	not determined, no side-chains					

Movie S1. Interpolation between three rotary states of V-ATPase.

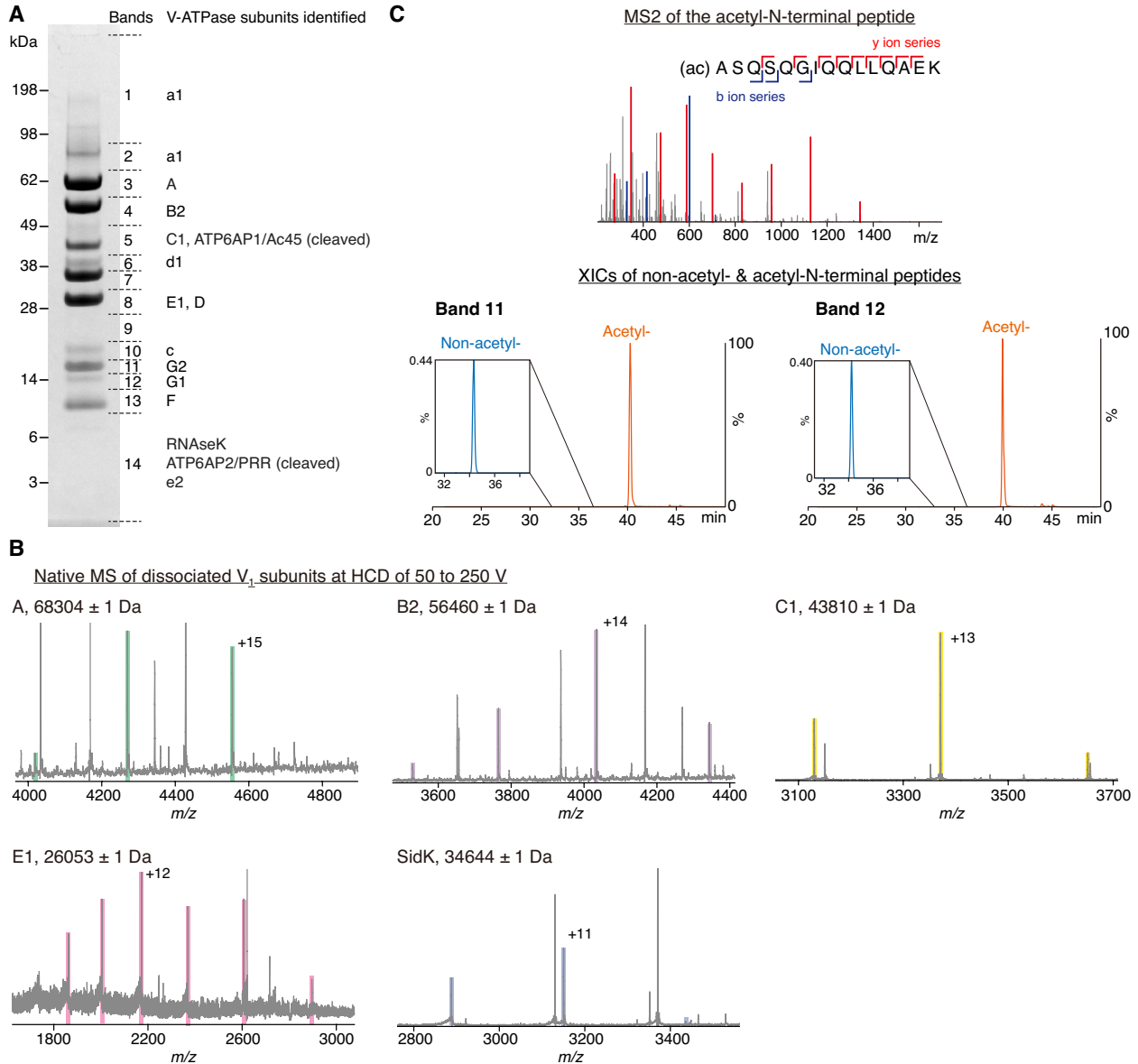


Fig. S1. Proteomic and native mass spectrometry. (A) SDS-PAGE of purified V-ATPase indicating where the gel was cut into fourteen bands for enzymatic digestion. The V-ATPase subunits identified by trypsin- or chymotrypsin-digestion of each gel band are indicated to the right. (B) Native mass spectra of V_1 subunits following dissociation at a higher-energy collisional (HCD) voltage of 50 to 250 V. The charge state for one peak per subunit is indicated. (C) Mass spectrum after fragmentation (MS2, *top*) of the N-terminal peptide that is common to both subunits G1 and G2 showing that it is acetylated, and extracted ion chromatograms (XICs, *bottom*) of the N-terminal peptide from subunit G2 (band 11) and subunit G1 (band 12) showing that the acetylated N-terminal peptides are more abundant than non-acetylated N-terminal peptides.

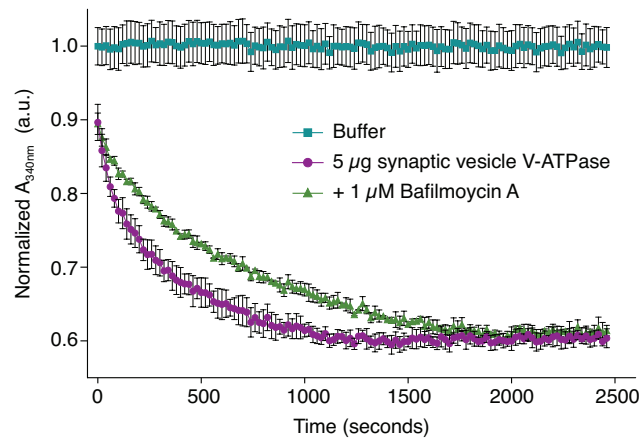


Fig. S2. Representative V-ATPase activity assay. ATP hydrolysis in an enzyme-coupled assay with an ATP-regenerating system showed a decreasing activity during (*purple circles*) that was only partially inhibited by bafilomycin a-1 at 1 μ M (*green triangles*). Data are normalized to buffer control (*teal squares*), and are shown as mean \pm SD, n = 3.

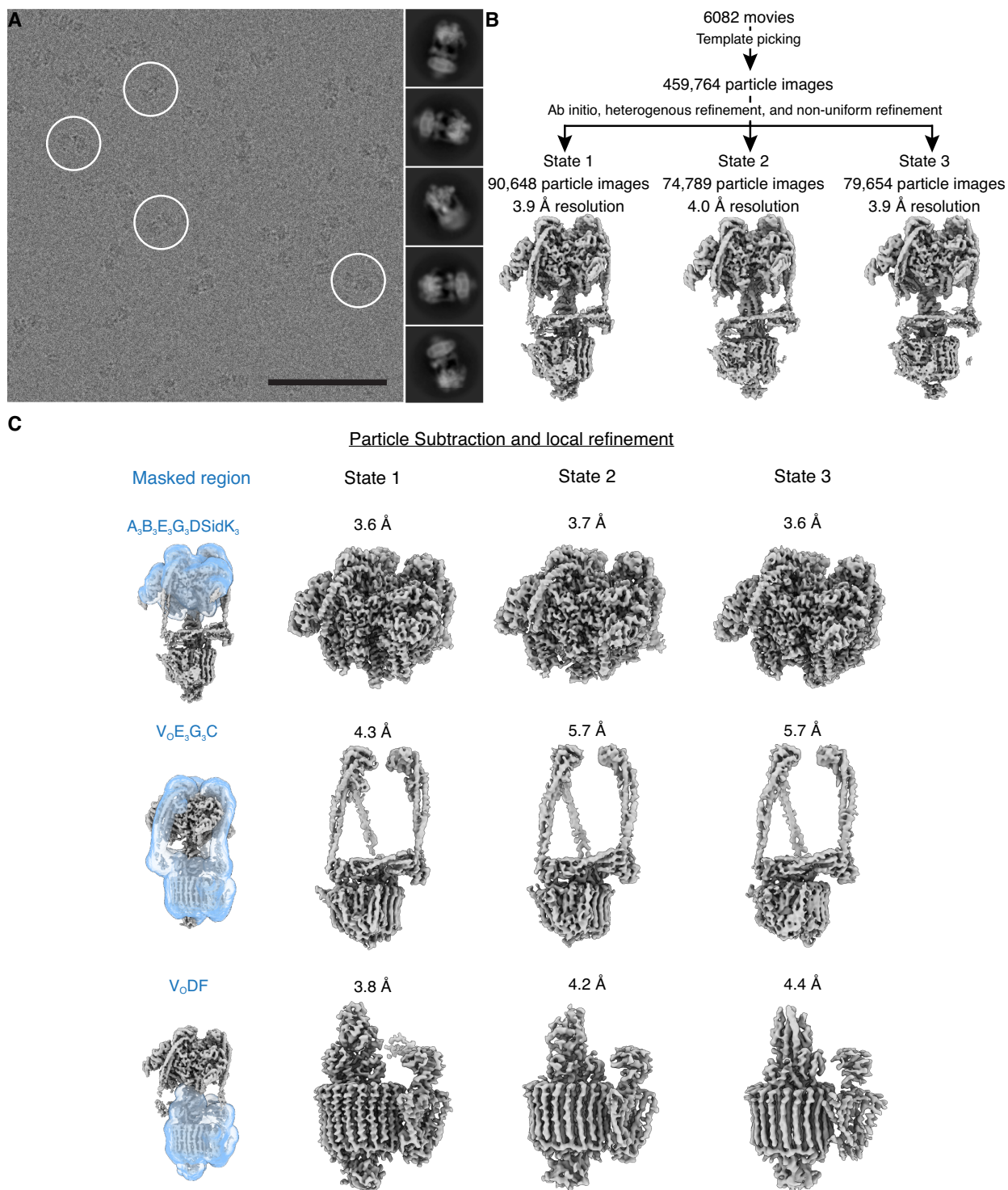


Fig. S3. CryoEM image analysis workflow. (A) Representative micrograph and class average images of V-ATPase from brain. (B) Image processing workflow to separate different conformational states. (C) Image processing workflow for focused refinement calculations.

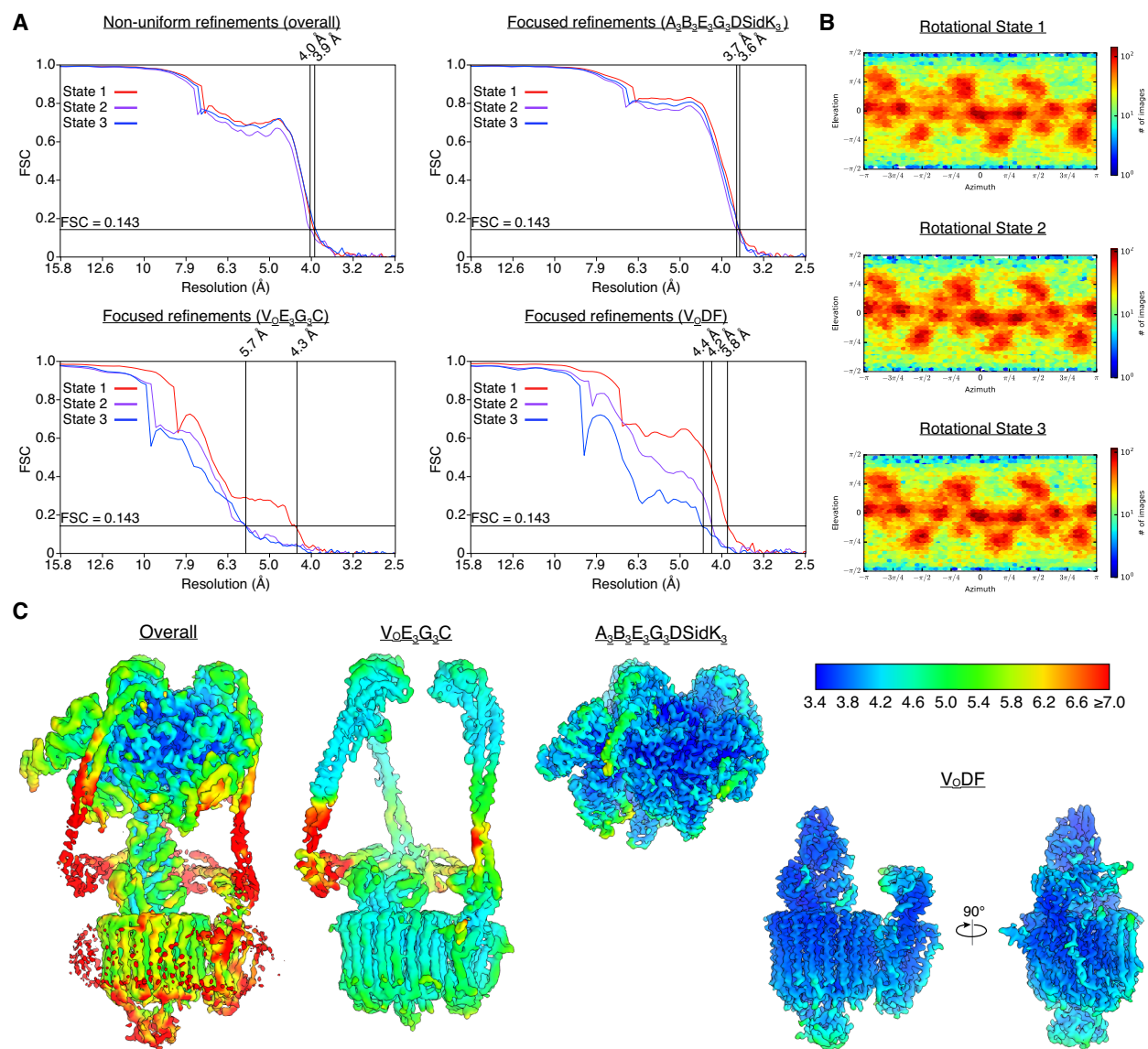


Fig. S4. CryoEM map validation. (A) Fourier shell correlation following map refinement. (B) Particle image orientation distribution demonstrates side views that lead to full coverage of Fourier space. (C) Local resolution maps following non-uniform and focused refinements.

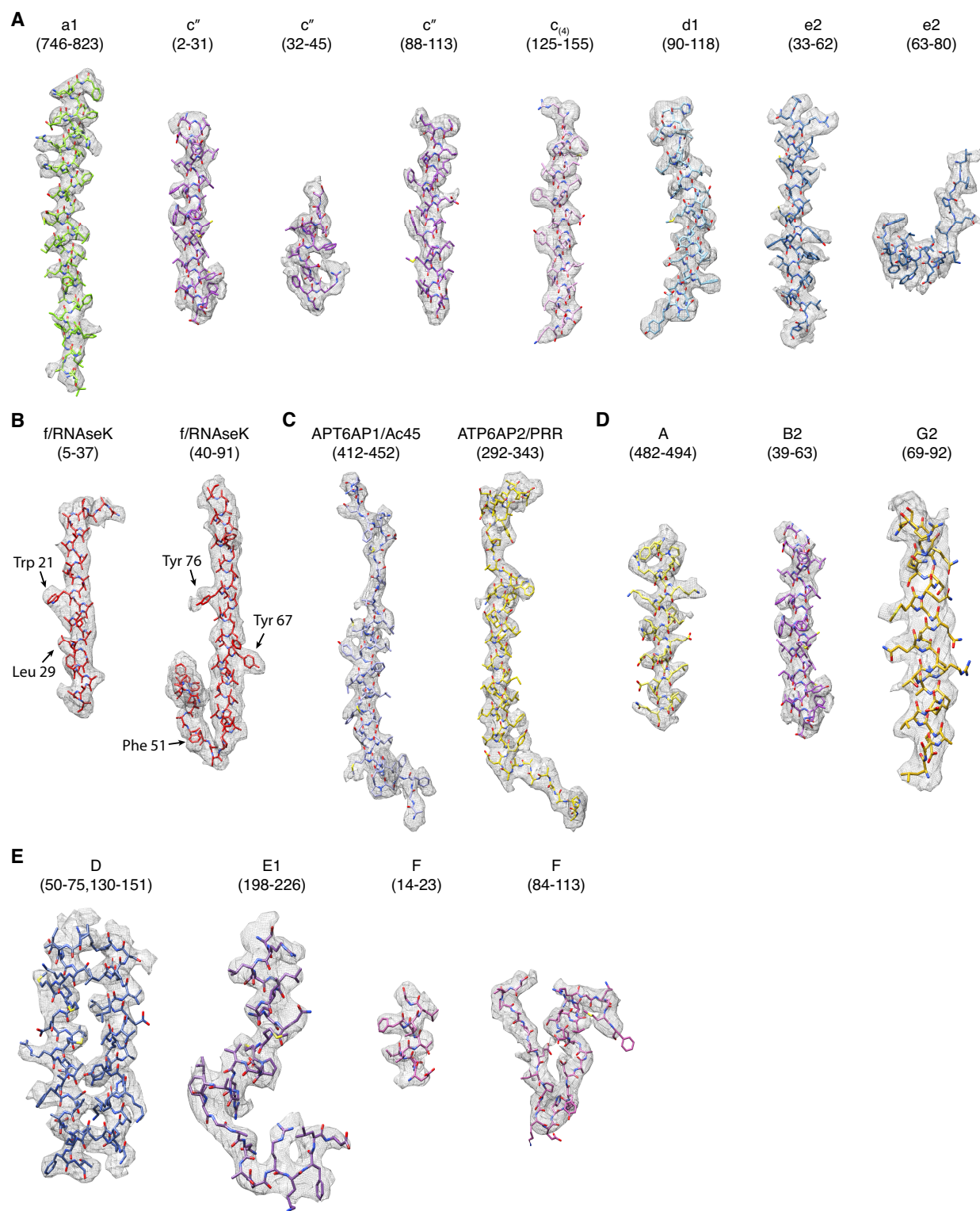


Fig. S5. Example model-in-map fit for representative map regions. (A) Model-in-map fit for subunits a1, c'', c₍₄₎, d1, and e2. **(B)** Suggested fit for RNaseK into subunit f density. **(C)** Fit for ATP6AP1/Ac45 and ATP6AP2/PRR. **(D)** Fit for subunits A, B2, and G2. **(E)** Fit for subunits D, E1, and F.

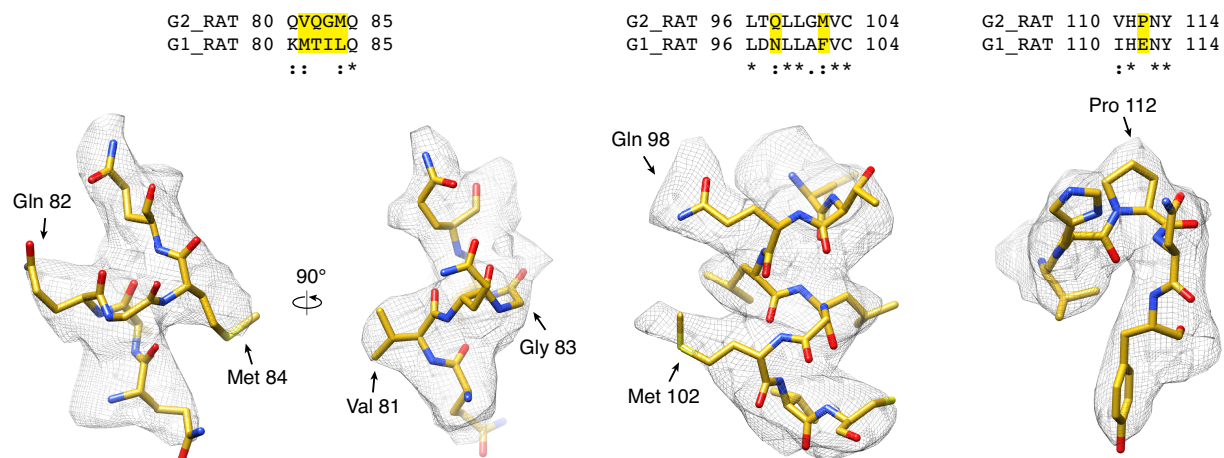


Fig. S6. Comparison of map density for isoforms of subunit G. Sequence alignment between rat G2 and rat G1, and fit for subunit G2. The indicated residues show well-resolved regions of the map where the density is more consistent with subunit G2 and not G1.

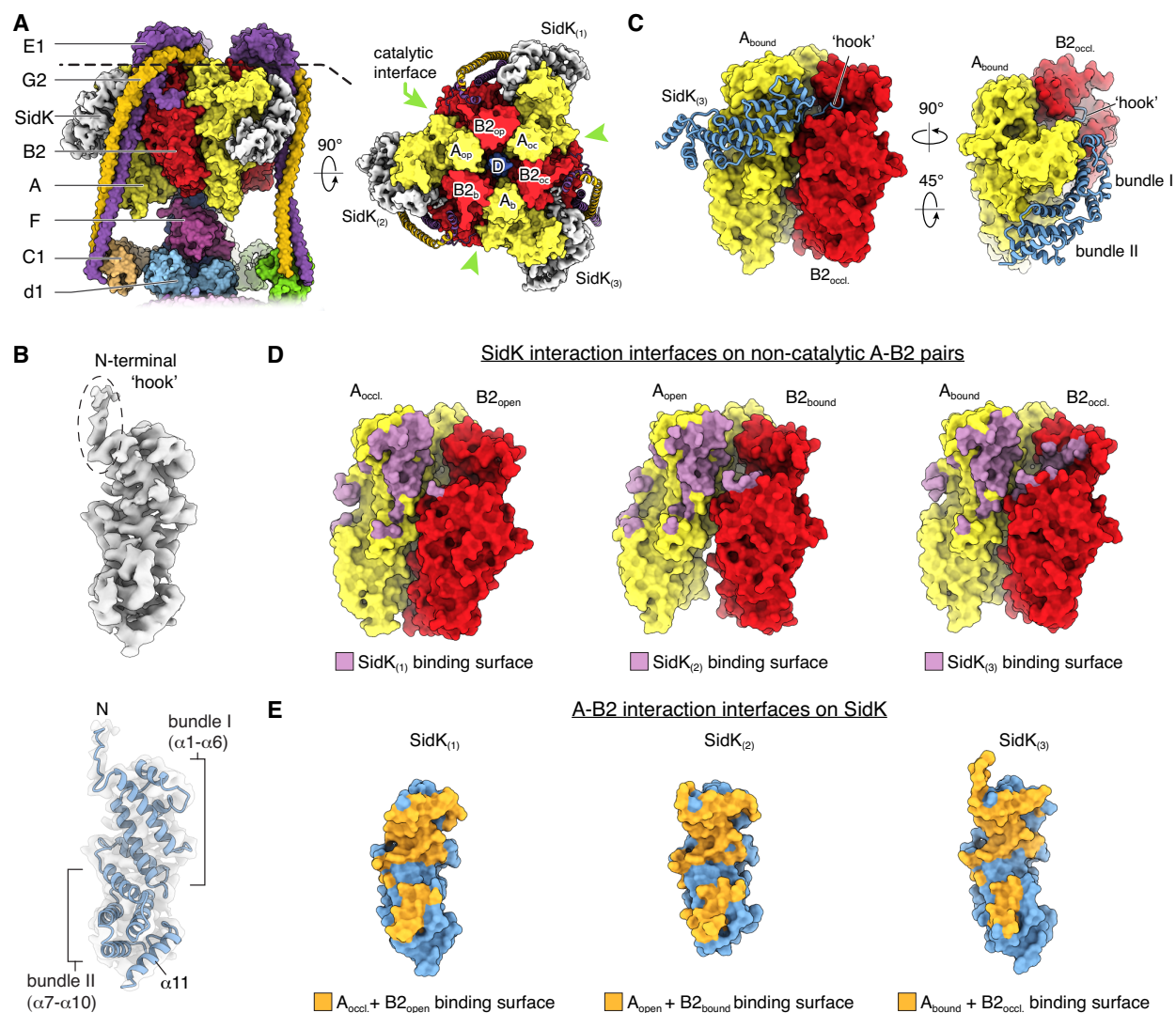


Fig. S7. Interaction of SidK with the V₁ region. (A) Surface representation of V₁ region with three molecules of SidK₁₋₂₇₈ shown in white. (B) SidK₁₋₂₇₈ density (*top*) and fit into the density (*bottom*). SidK₁₋₂₇₈ consists of two α -helical bundles and an N-terminal hook. (C) Interaction of SidK₍₃₎ with A_{bound} and B2_{occluded}. The α -helical bundles of SidK₁₋₂₇₈ wrap around a groove on subunit A while the N-terminal hook of SidK extends into a groove on subunit B2. (D) SidK interaction interface (*light purple*) with the corresponding non-catalytic A/B2 pairs. The interaction interface buries 1357, 1692, and 1829 Å² at SidK₍₁₎, SidK₍₂₎, and SidK₍₃₎, respectively. (E) A/B2 interaction interface on SidK (*orange*).

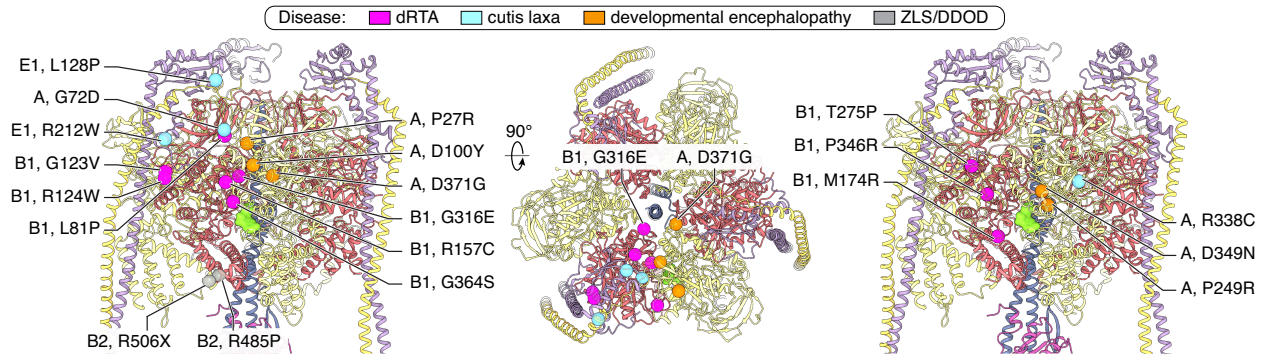


Fig. S8. Disease-associated mutations in subunits A, B, and E mapped onto the structure. Mutations associated with distal renal tubular acidosis (dRTA, *pink*), cutis laxa (*cyan*), developmental encephalopathy with epilepsy (*orange*), or Zimmermann-Laband syndrome (ZLS, *grey*), and dominant deafness-onychodystrophy syndrome (DDOD, *grey*). The majority of the mutants lie on or near the surface of subunits and likely affect subunit interactions (*left and middle*).

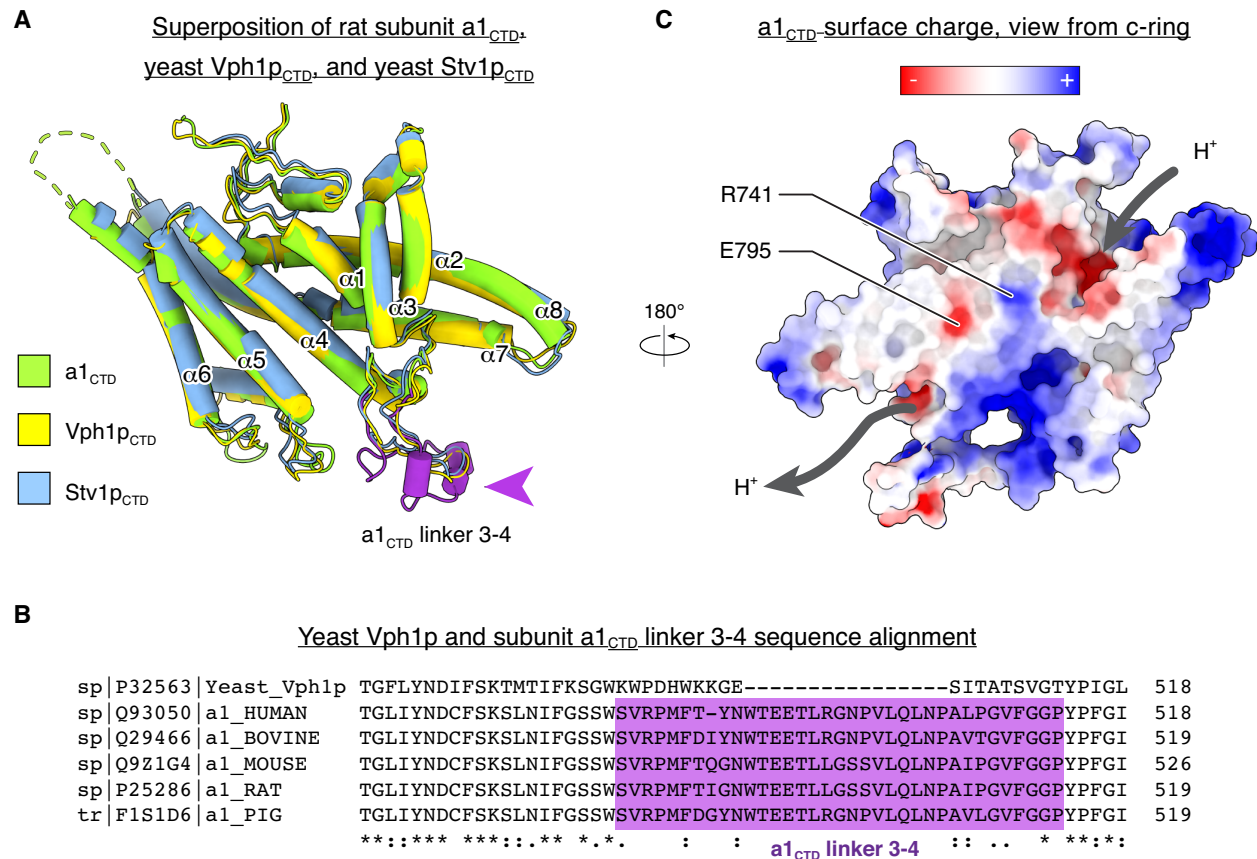
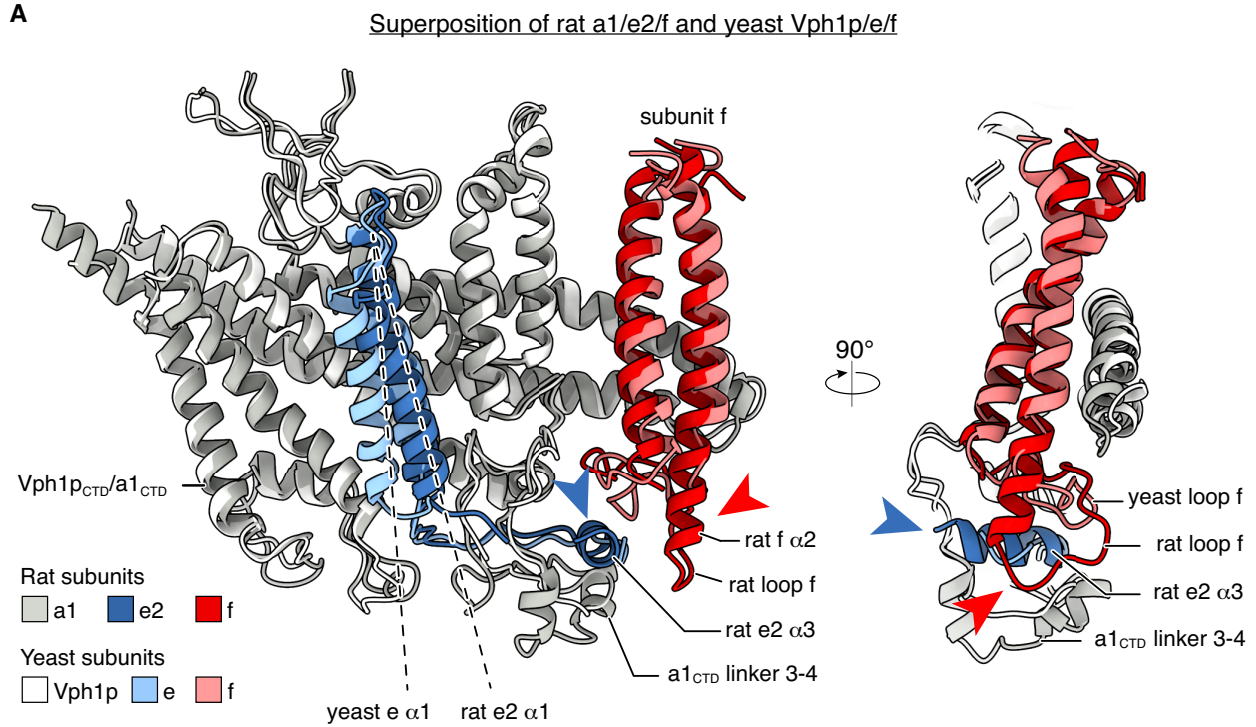


Fig. S9. Comparison of yeast and rat subunit a C-terminal domains. (A) Superposition of the C-terminal domains of yeast Vph1p (PDB 6O7T), yeast Stv1p (PDB 6O7U), and rat subunit a1. The luminal linker connecting $\alpha 3$ and $\alpha 4$ is coloured purple. The disordered loop connecting $\alpha 6$ and $\alpha 7$ is represented by a dashed line. (B) Sequence alignment for the luminal linker connecting $\alpha 3$ and $\alpha 4$ for mammalian subunit a1 and yeast Vph1p showing that the mammalian linker is longer. (C) C-terminal domain of subunit a1 coloured by surface electrostatic potential.




B Yeast Vma9p (e) and subunit e2 sequence alignment

sp Q3E7B6 Yeast_Vma9p	-----MSSFYTVVGVFIVVSAMSVLFWIMAPKNNQAVW	48
sp Q8NHE4 e2_HUMAN	MTAHSFALPVIIFTTFWGLVGI-----AGPWFVPKGPNRGVI	52
sp Q2KIB5 e2_BOVINE	MTAHSFALPVVIFTTFWGLIGI-----AGPWFVPKGPNRGVI	52
sp Q91XE7 e2_MOUSE	MTAHSFALPVIIFTTFWGLIGI-----AGPWFVPKGPNRGVI	52
sp Q5EB76 e2_RAT	MTAHSFALPVIIFTTFWGLIGI-----AGPWFVPKGPNRGVI	52
	:::* :::* . *:: *:.*	
sp Q3E7B6 Yeast_Vma9p	RSTVILTLAMMFLMWAITFLCQLHPLVAPRRSDLRPEFAE*---	73
sp Q8NHE4 e2_HUMAN	ITMLVATAVCCYLFWLIAILAQLNPLFGPQLKNETIWYVRFLWE	81
sp Q2KIB5 e2_BOVINE	ITMLVATAVCCYLFWLIAILAQLNPLFGPQLKNETIWYVRFLWE	81
sp Q91XE7 e2_MOUSE	ITMLVATAVCCYLFWLIAILAQLNPLFGPQLKNETIWYVRFLWE	81
sp Q5EB76 e2_RAT	ITMLVATAVCCYLFWLIAILAQLNPLFGPQLKNETIWYVRFLWE	81
	: : : * . :*:* *:*:*:*:*:*:* : : : e2 α 3	

Fig. S10. Comparison of yeast and rat subunits e and f. (A) Superposition of yeast subunits Vph1p_{CTD}, e, and f (from PDB 6C6L) and rat subunits a1_{CTD}, e2, and f. Rat e2 helix α 1 occupies a different position than α 1 in yeast subunit e (*dashed lines*). The C terminus of rat e2 contains a short helix (α 3, *blue arrowhead*) that is encircled by a1_{CTD} linker 3-4 and the luminal loop of rat subunit f. The luminal region of rat subunit f (helix α 2 and loop) is extended compared to yeast subunit f (*red arrowhead*). (B) Sequence alignment between the indicated mammalian subunit e2 sequences and yeast Vma9p (subunit e). The region encoding rat e2 α 3 is highlighted.

A

PSI-BLAST search result with yeast subunit f (YPR170W-B)

YPR170W-B	10	AWCCTVLSAFGVVILSVIAHLFNTNHESFVGSIDPDPEDGP-----AVAHTVYLAALVYLVF--FVFCGFQVYLARRK	79
		A C VLSA+GV++L ++ FN + + + D E+GP V++ ++AA +YL+ F FC QV L +RK	
Rat RNaseK	12	AACGIVLSAWGVIMLIMLGIFFNVHSAVLIEDVVPFTEKDFENGFPQNIYNLYEQVSYNCFIAAGLYLLGGFSPFC--QVRLNKRK	93
Modelled			

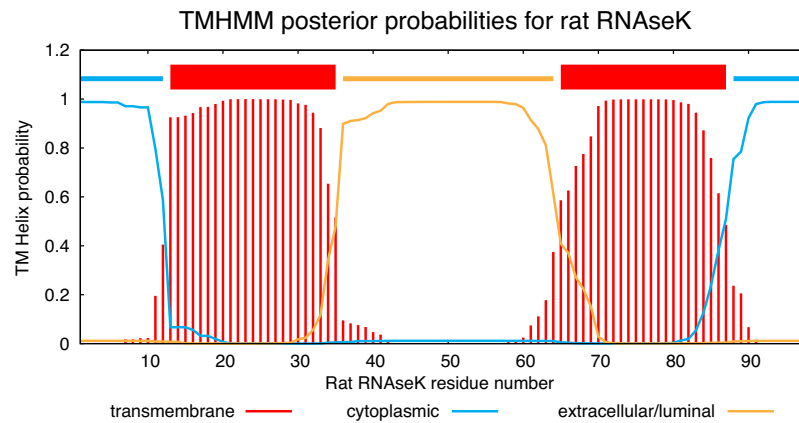
B

Fig. S11. RNaseK/subunit f alignment. (A) PSI-BLAST search result using yeast subunit f (YPR170W-B) as a query suggesting RNaseK as the mammalian homolog of yeast subunit f. Secondary structure of the RNaseK residues modelled into the rat subunit f cryoEM density are indicated. (B) Plot of transmembrane α -helical probability versus residue number for rat RNaseK, determined with TMHMM Server v. 2.0 (<http://www.cbs.dtu.dk/services/TMHMM/>).

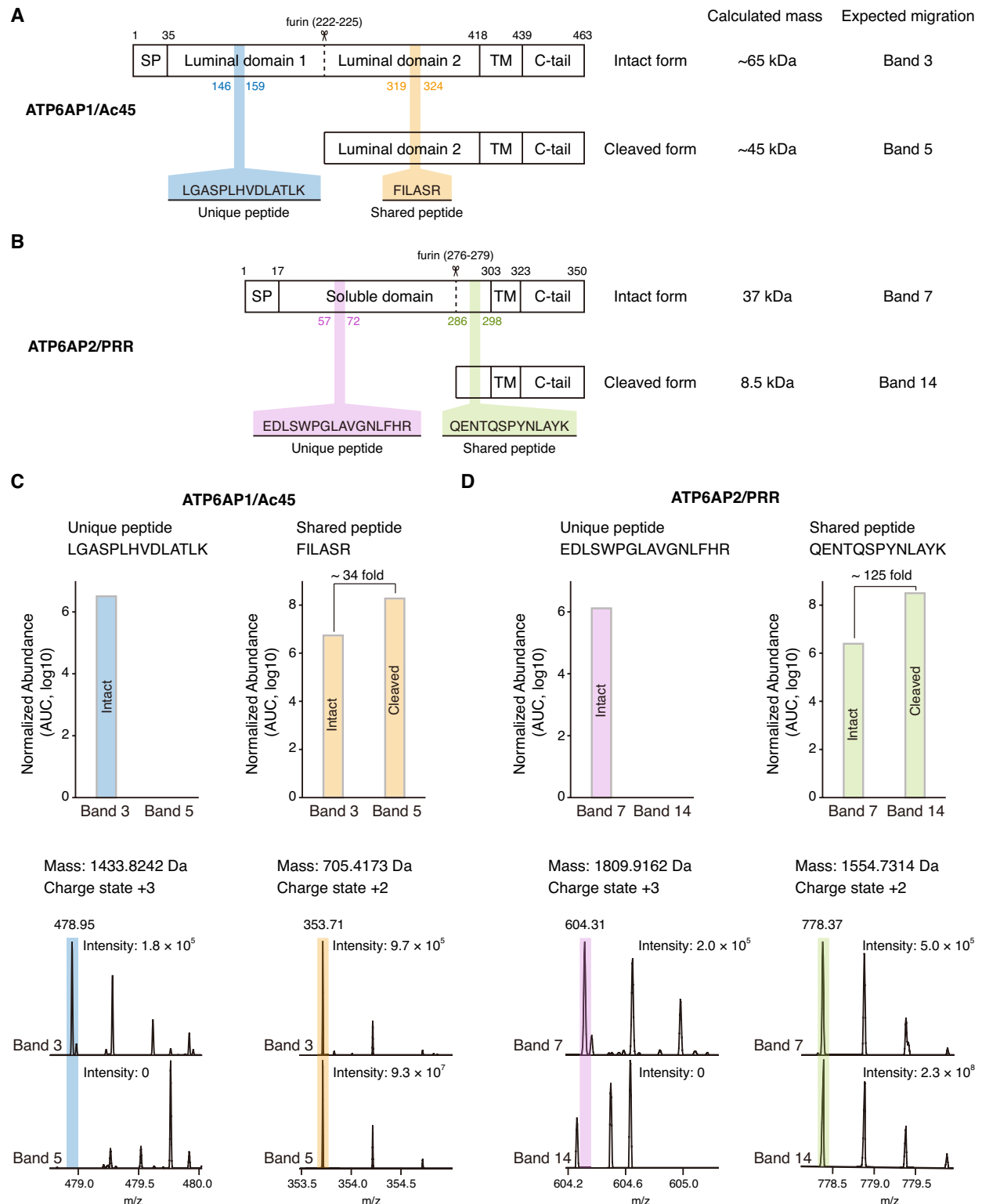


Fig. S12. Semi-quantitative mass spectrometry. (A) Consistent with previous SDS-PAGE (45), intact and cleaved ATP6AP1/Ac45 are found in gel Band 3 and 5, respectively. The ATP6AP1/Ac45 peptide FILASR is found in both the intact (Band 3) and cleaved (Band 5) protein while the peptide LGASPLHVDLTLK is found only in intact ATP6AP1/Ac45 (Band

3). The calculated masses of intact ATP6AP1/Ac45 does not include the signal peptide (SP). **(B)** Consistent with previous SDS-PAGE (13), intact and cleaved ATP6AP2/PRR are found in gel Bands 7 and 14, respectively. The peptide QENTQSPYNLAYK is found in both the intact (Band 7) and cleaved (Band 14) protein while the peptide EDLSWPGLAVGNLFHR is found only in intact ATP6AP2/PRR (Band 7). The calculated mass of intact ATP6AP2/PRR does not include the signal peptide (SP) and accounts for glycosylation of luminal domain 2 (45). **(C)** Extracted ion chromatogram (*bottom*) and normalized abundance (*top*) for the peptide FILASR, showing that this peptide is ~ 34-fold more abundant in Band 5 than in Band 3, suggesting that the cleaved protein is more abundant than the intact protein in the V-ATPase preparation. As a control, the peptide LGASPLHVDLATLK is only detected in Band 3, corresponding to the intact protein. AUC, area under the curve. **(D)** The normalized abundance of peptide QENTQSPYNLAYK is ~125-fold more in Band 14 than in Band 7, suggesting that the cleaved form of ATP6AP2/PRR is more abundant in the preparation. As a control, the peptide EDLSWPGLAVGNLFHR is only detected in Band 7, where the intact ATP6AP2/PRR is expected on the gel.

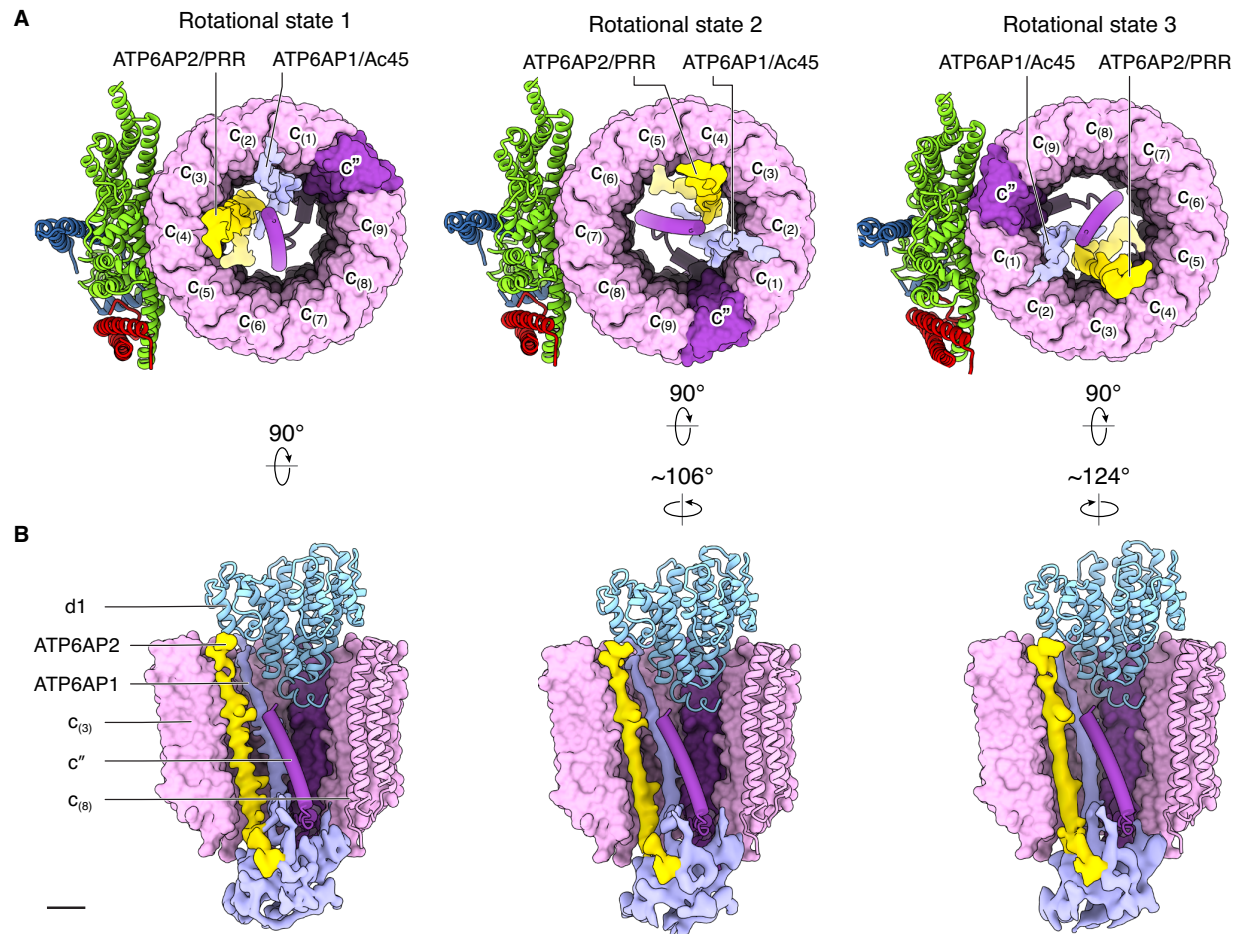


Fig. S13. Conformations of subunits d1, c'', ATP6AP/Ac45, and ATP6AP2/PRR in rotational states 2 and 3. (A) Vo region (viewed from V₁ towards the membrane) for each rotary state, with subunits a_{1NTD} and d1 removed. **(B)** Side view of subunits d1, c₍₈₎, c'', ATP6AP1/Ac45, and ATP6AP2/PRR in the different rotary states. Scale bar, 10 Å.

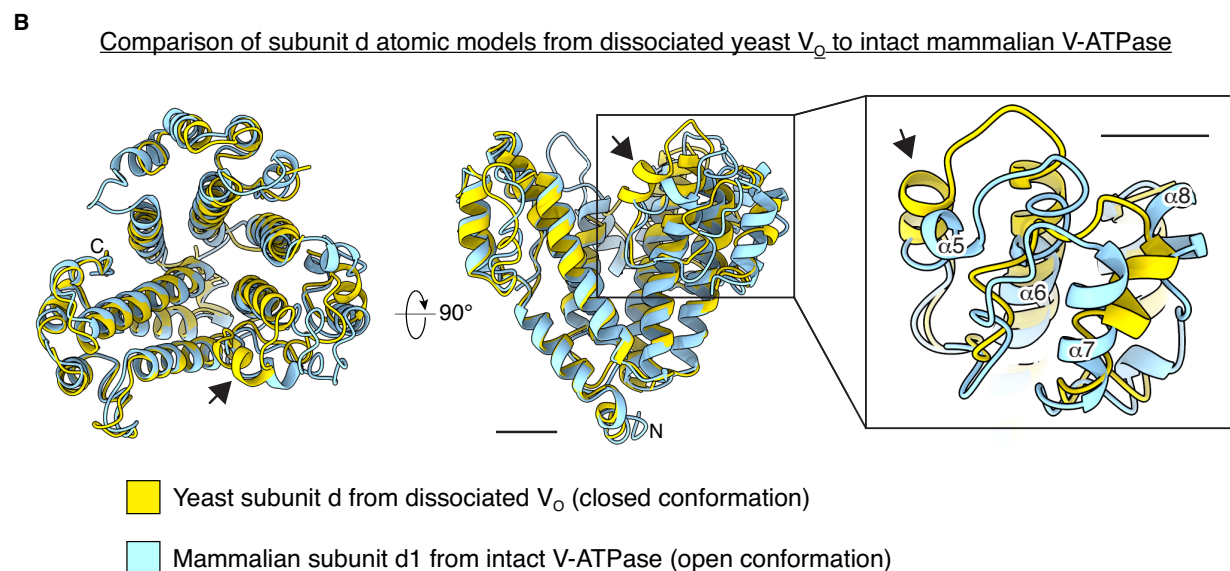
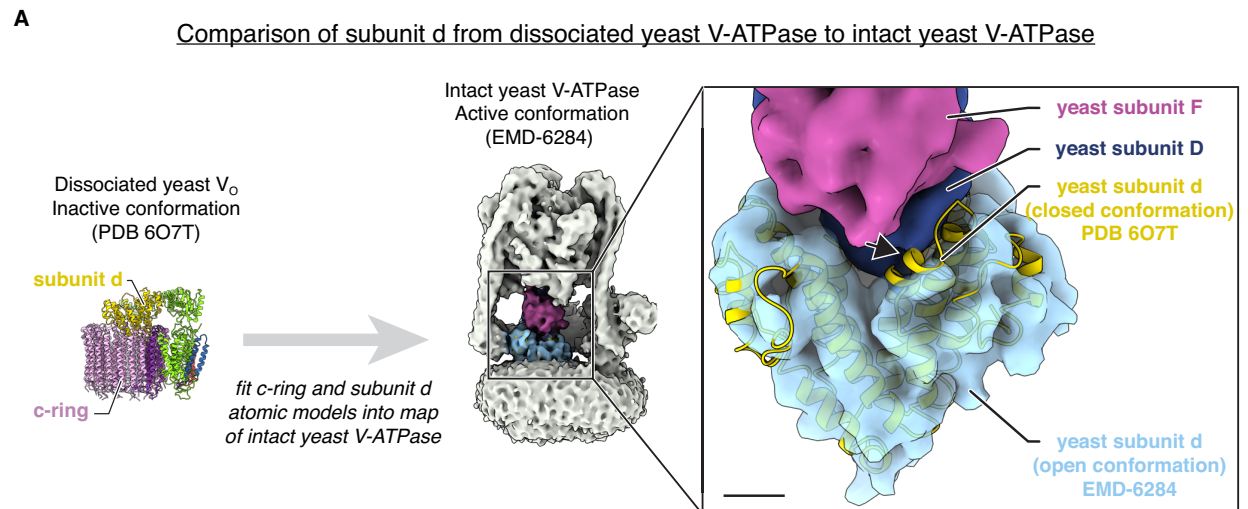


Fig. S14. Subunit d adopts different conformations in intact V-ATPase and dissociated V₀ region. (A) Subunit d and the c-ring from dissociated yeast V₀ (PDB 6O7T), which is in an inhibited conformation, were fit into the cryoEM map of intact yeast V-ATPase (EMD-6284). A close-up view of the fit shows that subunit d adopts a more closed conformation in the dissociated V₀ region (*yellow ribbon*) than in intact V-ATPase (*semi-transparent cyan surface*). An α -helix from subunit d in its conformation from the dissociated V₀ region clashes with subunit D from intact yeast V-ATPase (*blue surface*). Scale bar, 10 Å. (B) Superposition of subunit d from the dissociated yeast V₀ region and rat subunit d1 (RMSD 1 Å) shows that the rat subunit d1 from the intact V-ATPase is also in a more open conformation than yeast subunit d from the dissociated V₀ complex. The close-up shows that $\alpha 5$ from subunit d moves by ~ 7 Å towards the central axis of the protein. Scale bar, 10 Å.

References and notes:

57. C. R. Marr, S. Benlekber, J. L. Rubinstein, Fabrication of carbon films with approximately 500 nm holes for cryo-EM with a direct detector device. *J Struct Biol.* **185**, 42–47 (2014).
58. C. J. Russo, L. A. Passmore, Ultrastable gold substrates for electron cryomicroscopy. *Science (80-.).* **346**, 1377–1380 (2014).
59. J. R. Meyerson, P. Rao, J. Kumar, S. Chittori, S. Banerjee, J. Pierson, M. L. Mayer, S. Subramaniam, Self-assembled monolayers improve protein distribution on holey carbon cryo-EM supports. *Sci. Rep.* **4**, 7084 (2014).
60. W. F. Tivol, A. Briegel, G. J. Jensen, An improved cryogen for plunge freezing. *Microsc. Microanal.* **14**, 375–379 (2008).
61. A. Punjani, J. L. Rubinstein, D. J. Fleet, M. A. Brubaker, cryoSPARC: Algorithms for rapid unsupervised cryo-EM structure determination. *Nat. Methods.* **14** (2017), doi:10.1038/nmeth.4169.
62. J. L. Rubinstein, M. A. Brubaker, Alignment of cryo-EM movies of individual particles by optimization of image translations. *J. Struct. Biol.* **192**, 1–11 (2015).
63. A. Rohou, N. Grigorieff, CTFFIND4: Fast and accurate defocus estimation from electron micrographs. *J. Struct. Biol.*, 5–10 (2015).
64. X. C. Bai, E. Rajendra, G. Yang, Y. Shi, S. H. W. Scheres, Sampling the conformational space of the catalytic subunit of human g-secretase. *Elife.* **4**, 1–19 (2015).
65. E. F. Pettersen, T. D. Goddard, C. C. Huang, G. S. Couch, D. M. Greenblatt, E. C. Meng, T. E. Ferrin, UCSF Chimera - A visualization system for exploratory research and analysis. *J. Comput. Chem.* **25**, 1605–1612 (2004).
66. P. Emsley, K. Cowtan, Coot: Model-building tools for molecular graphics. *Acta Crystallogr. Sect. D Biol. Crystallogr.* **60**, 2126–2132 (2004).
67. O. Drory, F. Frolow, N. Nelson, Crystal structure of yeast V-ATPase subunit C reveals its stator function. *EMBO Rep.* **5**, 1148–1152 (2004).
68. R. A. Oot, L. S. Huang, E. A. Berry, S. Wilkens, Crystal structure of the yeast vacuolar ATPase heterotrimeric EGC(head) peripheral stalk complex. *Structure.* **20**, 1881–1892 (2012).
69. G. Bunkoczi, R. J. Read, Improvement of molecular-replacement models with Sculptor. *Acta Crystallogr D Biol Crystallogr.* **4**, 303–312 (2011).
70. A. Waterhouse, M. Bertoni, S. Bienert, G. Studer, G. Tauriello, R. Gumienny, F. T. Heer, T. A. P. de Beer, C. Rempfer, L. Bordoli, R. Lepore, T. Schwede, SWISS-MODEL: homology modelling of protein structures and complexes. *Nucleic Acids Res.* **46**, 296–303 (2018).
71. R. Y. Wang, Y. Song, B. A. Barad, Y. Cheng, J. S. Fraser, F. Dimaio, Automated structure refinement of macromolecular assemblies from cryo-EM maps using Rosetta. *Elife.* **5**, e17219 (2016).
72. V. B. Chen, W. B. Arendall, J. J. Headd, D. A. Keedy, R. M. Immormino, G. J. Kapral, L. W. Murray, J. S. Richardson, D. C. Richardson, MolProbity: all-atom structure validation for macromolecular crystallography. *Acta Crystallogr. Sect. D Biol. Crystallogr.* **66**, 12–21 (2010).
73. B. A. Barad, N. Echols, R. Y. R. Wang, Y. Cheng, F. Dimaio, P. D. Adams, J. S. Fraser, EMRinger: Side chain-directed model and map validation for 3D cryo-electron microscopy. *Nat. Methods.* **12**, 943–946 (2015).

74. T. D. Goddard, C. C. Huang, E. C. Meng, E. F. Pettersen, G. S. Couch, J. H. Morris, T. E. Ferrin, UCSF ChimeraX: Meeting modern challenges in visualization and analysis. *Protein Sci.* **27**, 14–25 (2018).
75. A. Shevchenko, M. Wilm, O. Vorm, M. Mann, Mass spectrometric sequencing of proteins from silver-stained polyacrylamide gels. *Anal. Chem.* **68**, 850–858 (1996).
76. J. V. Olsen, L. M. F. de Godoy, G. Li, B. Macek, P. Mortensen, R. Pesch, A. Makarov, O. Lange, S. Horning, M. Mann, Parts per million mass accuracy on an orbitrap mass spectrometer via lock mass injection into a C-trap. *Mol. Cell. Proteomics.* **4**, 2010–2021 (2005).
77. S. F. Altschul, T. L. Madden, A. A. Schäffer, J. Zhang, Z. Zhang, W. Miller, D. J. Lipman, Gapped BLAST and PSI-BLAST: a new generation of protein database search programs. *Nucleic Acids Res.* **25**, 3389–3402 (1997).
78. Y. Ishihama, Y. Oda, T. Tabata, T. Sato, T. Nagasu, J. Rappsilber, M. Mann, Exponentially modified protein abundance index (emPAI) for estimation of absolute protein amount in proteomics by the number of sequenced peptides per protein. *Mol. Cell. Proteomics.* **4**, 1265–1272 (2005).